Inorganic Chemistry

Article

pubs.acs.org/IC

Strong Second Harmonic Generation (SHG) Originating from Combined Second-Order Jahn–Teller (SOJT) Distortive Cations in a New Noncentrosymmetric Tellurite, $InNb(TeO_4)_2$

Yeong Hun Kim, Dong Woo Lee, and Kang Min Ok*

Department of Chemistry, Chung-Ang University, 84 Heukseok-ro, Dongjak-gu, Seoul 156-756, Korea

Supporting Information

ABSTRACT: Pure polycrystalline bulk samples and single crystals of a novel polar noncentrosymmetric (NCS) indium niobium tellurium oxide, $InNb(TeO_4)_2$, have been synthesized through solid-state reactions with In_2O_3, Nb_2O_5, and TeO_2. $InNb(TeO_4)_2$ exhibits a three-dimensional structural backbone consisting of layers of corner-shared InO_6 octahedra, layers of corner-shared NbO_6 octahedra, and chains of corner-shared TeO_4 polyhedra. The infrared spectrum shows In–O, Nb–O, and Te–O vibrations, and the UV–vis diffuse reflectance spectrum shows a band gap of 3.5 eV for the reported material. Thermal analysis indicates that $InNb(TeO_4)_2$ is thermally stable to 740 °C. Powder second-order nonlinear optical (NLO) measurements reveal that $InNb(TeO_4)_2$ has a strong second harmonic generation (SHG) efficiency, 100 times that of α-SiO_2. A detailed structural examination indicates that the strong SHG is due to the combined net polarization originating from the distorted environment of second-order Jahn–Teller (SOJT) cations such as Nb^{5+} and Te^{4+}. Elemental analysis, the magnitude of distortion, and calculations of dipole moments for $InNb(TeO_4)_2$ are also presented.

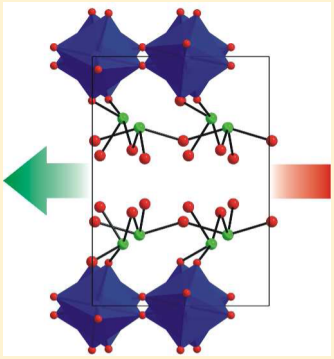

INTRODUCTION

Materials exhibiting macroscopic noncentrosymmetric (NCS) structures have been drawing enormous attention attributable to their extremely important characteristics such as piezoelectric, ferroelectric, pyroelectric, and second-order nonlinear optical (NLO) properties.[1−7] Thus, synthetic chemists continuously have made every effort to discover novel NCS compounds with superior performance by amalgamating cations with an unsymmetrical arrangement of environments. For oxide materials, asymmetric distorted coordination moieties are considered to be the consequence of second-order Jahn–Teller (SOJT) effects.[8−14] Two classes of cations, i.e., octahedrally linked d^0 transition metals (Zr^{4+}, V^{5+}, Ta^{5+}, W^{6+}, etc.) and lone pair cations (Pb^{2+}, Bi^{3+}, Se^{4+}, etc.) are considered to be inherently in asymmetric polar environments through the SOJT. For d^0 transition-metal cations with octahedral coordination, the SOJT distortions usually arise when the vacant d orbitals in metals combine with the occupied p orbitals in ligands. These octahedral distortions in many cases are found along one of three directions: in the direction of a corner (tetragonally along the local C_4 axis), an edge (orthorhombically along the local C_2 axis), or a face (rhombohedrally along the local C_3 axis).[15] Meanwhile, the strong mutual influence between the p orbitals of the anion and the s and p orbitals of the cation should be critical for lone pair formation, although the case is more intricate.[16−22] A very common lone pair cation is normally observed in tellurites, i.e., oxides containing Te^{4+} cation. Tellurites are synthetically and structurally very versatile materials. The general starting compound, tellurium dioxide (TeO_2), has been employed extensively in the syntheses of many new tellurite materials, attributable to a lower melting point of 733 °C. The attainable temperature has enabled the material to be utilized for crystal growth as a flux.[23−26] In addition, TeO_2 can produce a variety of novel oxide materials, attributed to its excellent reactivities with most oxides.[27,28] Moreover, Te^{4+} can reveal variable coordination geometries such as square pyramidal, seesaw, and trigonal pyramidal.[29−31] Thus, if both lone pair cations and d^0 transition-metal cations are combined, asymmetric frameworks with rich structural chemistry would be possible.[32−35] Thus, we investigated the In^{3+}–Nb^{5+}–Te^{4+}–oxide system in an earnest manner and discovered a new NCS tellurite phase. So far, several ternary[36,37] and quaternary niobium tellurites including alkali,[38,39] alkaline earth,[40,41] bismuth,[42] and lanthanum[43] metals have been published. A series of stoichiometrically similar quaternary vanadium tellurites, $M^{3+}VTe_2O_8$ (M = In, Sc, Y), have been also found.[44−46] Among many, $Te_3Nb_2O_{11}$ exhibits a NCS space group, $P2_12_12$.[36] In this article, we report the preparation, structural determination, and second-order NLO properties of a novel polar indium niobium tellurite, $InNb(TeO_4)_2$. Thermal analysis, UV–vis diffuse reflectance spectroscopy, infrared spectroscopy, dipole moment calculations, and calculations of the magnitude of octahedral distortion are also reported. Furthermore, the origin of the observed strong SHG efficiency for the reported material will be discussed by analyzing the net polarization occurring from SOJT distortive cations, Nb^{5+} and Te^{4+}.

Received: February 24, 2014
Published: May 7, 2014

   dx.doi.org/10.1021/ic5004337 | Inorg. Chem. 2014, 53, 5240–5245

EXPERIMENTAL SECTION

Reagents. TeO_2 (Alfa Aesar, 98%), In_2O_3 (Alfa Aesar, 99.9%), and Nb_2O_5 (Alfa Aesar, 99.5%) were used in synthesis as received.

Synthesis. Single crystals of $InNb(TeO_4)_2$ were obtained by a standard solid-state reaction. A 0.083 g amount (3.00×10^{-4} mol) of In_2O_3, 0.080 g (3.00×10^{-4} mol) of Nb_2O_5, and 0.287 g (1.80×10^{-3} mol) of TeO_2 were mixed and ground intimately with a mortar and a pestle. After it was pressed into a pellet, the reaction mixture was placed in a quartz tube that was subsequently evacuated. The tube was evacuated for 15 min and subsequently sealed. The sealed tube containing the reaction mixture was heated to 800 °C for 48 h. After heating, the tube was cooled slowly to 550 °C at a rate of 6 °C h^{-1} and then quenched to room temperature. Light yellow crystals of $InNb(TeO_4)_2$ were obtained with unknown amorphous phases, since an excess amount of TeO_2 was used as a melt at high temperature. After the structure was determined by single-crystal X-ray diffraction, a bulk polycrystalline sample of $InNb(TeO_4)_2$ was prepared by a similar reaction using stoichiometric amounts of starting chemicals. A 0.555 g portion (2.00×10^{-3} mol) of In_2O_3, 0.532 g (2.00×10^{-3} mol) of Nb_2O_5, and 1.277 g (8.00×10^{-3} mol) of TeO_2 were ground for 15 min and introduced into a quartz tube that was then evacuated and sealed. The reaction mixture in a sealed tube was heated to 500, 600, 700, and 750 °C for 12 h with intermittent regrindings at each temperature. The resultant product was identified as a single phase on the basis of powder X-ray diffraction (XRD). As seen in PXRD data deposited in the Supporting Information, the pure bulk phase of $InNb(TeO_4)_2$ has been successfully synthesized.

Single-Crystal X-ray Diffraction. To determine the crystal structure of $InNb(TeO_4)_2$, standard crystallographic methods were employed. A pale yellow block crystal ($0.018 \times 0.022 \times 0.028$ mm^3) of $InNb(TeO_4)_2$ was selected for single-crystal data analysis. The diffraction data were collected at 298 K using a Bruker SMART BREEZE diffractometer using Mo Kα radiation. The data were obtained with scan widths of 0.30° and an exposure time of 10 s/frame using a narrow-frame method. To monitor crystal and instrument stability, the initial 50 frames were remeasured at the end of the data collection. All of the collected diffractions were integrated with the SAINT program.[47] The intensities were also corrected for air absorption, Lorentz factor, polarization, and absorption attributed to the deviation in the path length through the detector faceplate. The SADABS program was used for an absorption correction on the hemisphere of data.[48] The data were solved with SHELXS-97[49] and refined using SHELXL-97.[50] All calculations were carried out through the WinGX-98 crystallographic software package.[51] Summary of crystallographic information along with selected bond distances for $InNb(TeO_4)_2$ are provided in Tables 1 and 2. As seen in Table 1, the refined Flack parameter for $InNb(TeO_4)_2$ is −0.03(2).

Table 1. Crystallographic Data for $InNb(TeO_4)_2$

formula	$InNbTe_2O_8$
fw	590.93
space group	$Pca2_1$ (No. 29)
a (Å)	7.63610(10)
b (Å)	10.82980(10)
c (Å)	7.65640(10)
V (Å^3)	633.165(13)
Z	4
T (K)	298.0(2)
λ (Å)	0.71073
ρ_{calcd} (g cm^{-3})	6.199
μ (mm^{-1})	14.492
Flack param	−0.03(2)
$R(F)^a$	0.0141
$R_w(F_o^2)^b$	0.0295

$^aR(F) = \sum||F_o| - |F_c||/\sum|F_o|$. $^bR_w(F_o^2) = [\sum w(F_o^2 - F_c^2)^2/\sum w(F_o^2)^2]^{1/2}$.

Table 2. Selected Bond Distances (Å) for $InNb(TeO_4)_2$

In(1)−O(5)	2.167(3)	In(1)−O(7)	2.145(3)
In(1)−O(5)	2.276(3)	In(1)−O(8)	2.141(3)
In(1)−O(6)	2.191(3)	In(1)−O(8)	2.297(3)
Nb(1)−O(1)	1.987(3)	Nb(1)−O(3)	1.812(3)
Nb(1)−O(2)	1.852(4)	Nb(1)−O(3)	2.175(3)
Nb(1)−O(2)	2.097(4)	Nb(1)−O(4)	2.066(3)
Te(1)−O(1)	1.895(3)	Te(2)−O(6)	1.904(3)
Te(1)−O(4)	1.886(3)	Te(2)−O(7)	2.044(4)
Te(1)−O(5)	1.919(3)	Te(2)−O(7)	2.070(4)
Te(1)−O(6)	2.469(3)	Te(2)−O(8)	1.889(3)

Powder X-ray Diffraction. To monitor the phase purity of $InNb(TeO_4)_2$, a powder XRD pattern was obtained on a Bruker D8-Advance diffractometer (Cu Kα radiation) with 40 kV and 40 mA at room temperature. The sample holder was mounted with the powder sample and scanned in the 2θ range of 5−70° with a step time of 0.2 s and a step size of 0.02°. The measured PXRD data are in good agreement with the simulated pattern from the single-crystal model.

UV−Vis Diffuse Reflectance Spectroscopy. The UV−vis diffuse reflectance spectrum was recorded over the spectral range 200−2500 nm on a Varian Cary 500 scan UV−vis−NIR spectrophotometer at the Korea Photonics Technology Institute at room temperature. To change the reflectance spectrum to absorbance, the Kubelka−Munk function was employed.[52,53]

Infrared Spectroscopy. The infrared spectrum was obtained in the 400−4000 cm^{-1} range using a Thermo Scientific Nicolet 6700 FT-IR spectrometer with the sample embedded in a KBr matrix.

Thermal Analysis. Thermogravimetric analysis was carried out using a Setaram LABSYS TG-DTA thermogravimetric analyzer. The well-ground powder sample was placed in an alumina crucible and heated at a rate of 10 °C min^{-1} under flowing argon from ambient temperature to 1000 °C.

Second Harmonic Generation (SHG) Measurements. Powder SHG measurements on polycrystalline NCS $InNb(TeO_4)_2$ were carried out using 1064 nm radiation by a Kurtz-nonlinear optical (NLO) measurement system.[54] For the measurements, a DAWA Q-switched Nd:YAG laser working at 20 Hz was employed. Since SHG efficiencies for powder samples strongly depend on particle size, ground powder samples were graded into several different ranges of particle size (20−45, 45−63, 63−75, 75−90, 90−125, >125 μm). Also, crystalline α-SiO_2 and $LiNbO_3$ were sieved into the same particle size ranges in order to compare suitably with known SHG materials. Samples with particle size 45−63 μm were used to compare SHG intensities. Polycrystalline materials having distinct particle sizes were placed in individual capillary tubes. The reflected frequency-doubled SHG light (532 nm green) was gathered and detected by a photomultiplier tube (Hamamatsu). To detect only the frequency-doubled light, a narrow-pass interference filter (532 nm) was attached to the tube. To view the SHG signal, a digital oscilloscope (Tektronix TDS1032) was connected. A detailed statement of the equipment and the methodology has been reported.[6]

Scanning Electron Microscopy/Energy Dispersive Analysis by X-ray (SEM/EDAX). Hitachi S-3400N/Horiba Energy EX-250 instruments were used to obtain SEM/EDAX data. EDAX for $InNb(TeO_4)_2$ reveals an In/Nb/Te ratio of 1.0/0.8/1.9. The measured SEM/EDAX data can be found in the Supporting Information.

RESULTS AND DISCUSSION

Structure. $InNb(TeO_4)_2$ crystallizes in a polar non-centrosymmetric space group, $Pca2_1$ (No. 29). As seen in Figure 1, $InNb(TeO_4)_2$ reveals a three-dimensional framework composed of distorted InO_6, NbO_6, and TeO_4 polyhedra. A unique In^{3+} cation is in a deformed octahedral coordination moiety with six oxygen atoms. The O−In−O bond angles range

dx.doi.org/10.1021/ic5004337 | Inorg. Chem. 2014, 53, 5240−5245

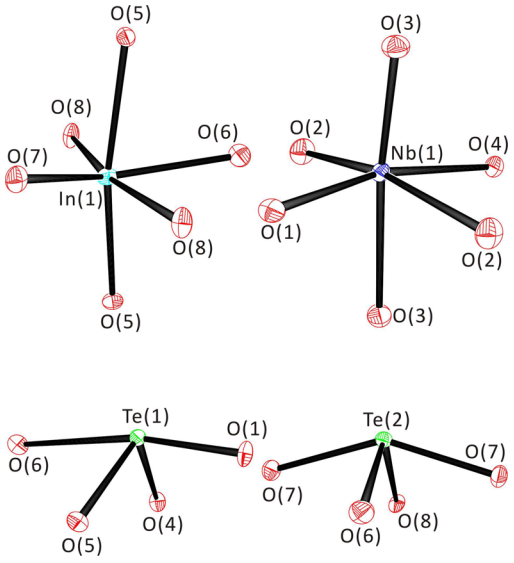

Figure 1. ORTEP drawing (50% probability ellipsoids) of InO_6, NbO_6, and TeO_4 polyhedra in $InNb(TeO_4)_2$.

from 67.82(13) to 170.21(16)°, and the In−O bond lengths range from 2.141(3) to 2.297(3) Å. The d^0 cation, Nb^{5+}, is also in a distorted-octahedral environment with six oxygen atoms. As seen in Figure 1, the unique Nb^{5+} cation exhibits a local C_3 distortion in the direction of a face of the NbO_6 octahedron, which generates three long (2.066(3)−2.175(3) Å) and three short (1.812(3)−1.987(3) Å) Nb−O bond lengths. Also, the O−Nb−O angles range from 79.94(16) to 173.0(3)°, as anticipated from the distorted coordination moiety. In an asymmetric unit, there are two unique Te^{4+} cations where both $Te(1)^{4+}$ and $Te(2)^{4+}$ are connected to four oxygen atoms. However, the coordination modes found in two unique Te^{4+} cations are different: $Te(1)^{4+}$ reveals one very long (2.469(3) Å) and three short (1.886(3)−1.919(3) Å) Te−O bond distances, whereas, $Te(2)^{4+}$ exhibits two long (2.044(4) and 2.070(4) Å) and two short (1.889(3) and 1.904(3) Å) Te−O bond lengths in seesaw environments. The observed O−Te−O bond angles range from 75.95(12) to 168.06(12)°.

The structural backbone of $InNb(TeO_4)_2$ mainly consists of chains of corner-shared TeO_4 polyhedra, layers of corner-shared InO_6 octahedra, and layers of corner-shared NbO_6 octahedra. As can be seen in Figure 2a, each InO_6 octahedron

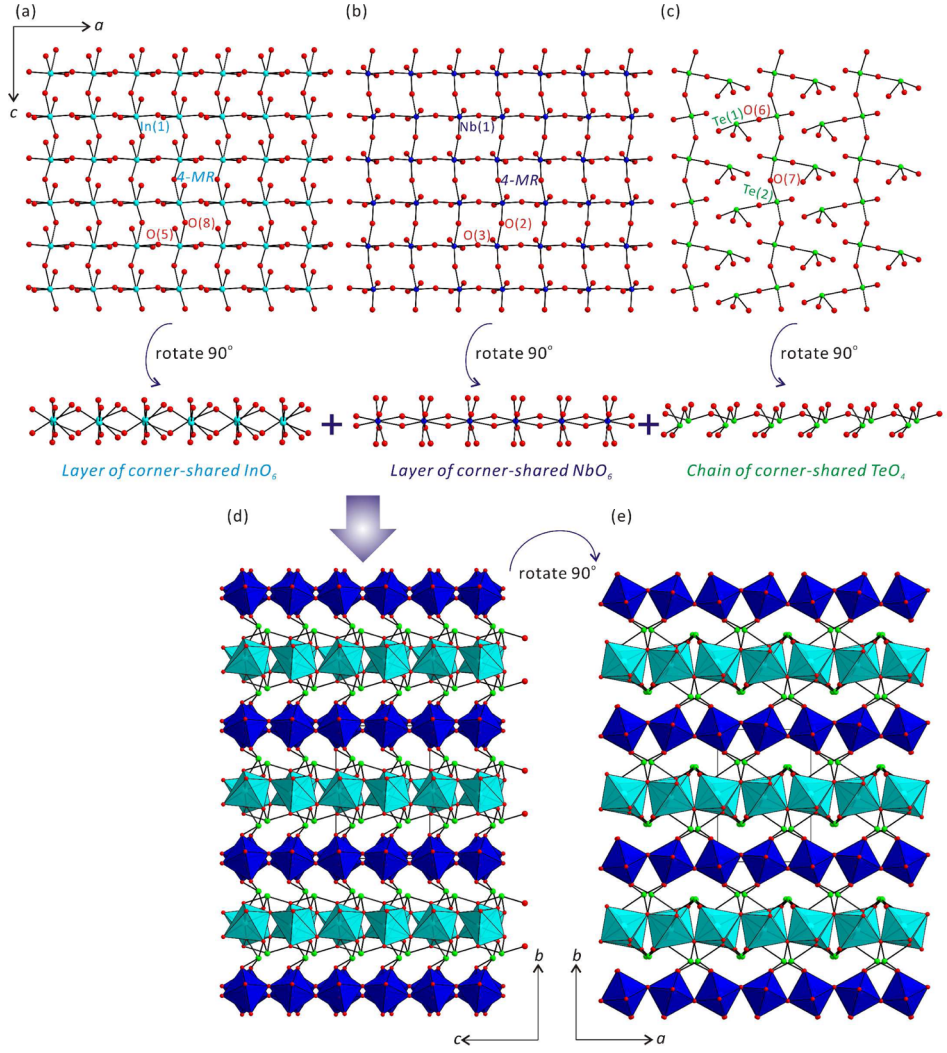

Figure 2. (a−c) Ball-and-stick representations of (a) a layer of corner-shared InO_6 octahedra, (b) a layer of corner-shared NbO_6 octahedra, and (c) a chain of corner-shared TeO_4 polyhedra in $InNb(TeO_4)_2$ (cyan, In; blue, Nb; green, Te; red, O). (d, e) Polyhedral models representing a complete three-dimensional framework of $InNb(TeO_4)_2$ in the (d) *bc* plane and (e) *ab* plane.

dx.doi.org/10.1021/ic5004337 | *Inorg. Chem.* 2014, 53, 5240−5245

shares its corners with O(5) and O(8) and constructs a layer in the *ac* plane. Through the corner sharing of InO_6 octahedra, four-membered rings (4MRs) are obtained. Also, along the [001] and [100] directions, the distorted NbO_6 share their corners with O(2) and O(3), respectively, which results in another layer of vertex-shared NbO_6 octahedra in the *ac* plane. As seen in Figure 2b, other 4MRs composed of NbO_6 octahedra are also observed in the *ac* plane. Meanwhile, each $Te(2)O_4$ polyhedron shares its vertices through O(7) and constructs infinite chains parallel to the *c* direction. Furthermore, the $Te(1)O_4$ groups are connected to the chains of corner-shared $Te(2)O_4$ polyhedra through O(6) along the approximate [100] and [−100] directions. In other words, infinite chains of corner-shared $Te(2)O_4$ groups are fitted by the $Te(1)O_4$ studs in the *ac* plane (see Figure 2c). Once the layers and chains are combined, a 3D framework of $InNb(TeO_4)_2$ is fully developed, as seen in Figure 2d,e. One can notice that, while the $Te(1)O_4$ groups work as interlayer linkers, the $Te(2)O_4$ polyhedra serve as intralayer linkers. The structure of $InNb(TeO_4)_2$ can be delineated as an $\{[InO_{6/3}]^-[NbO_{6/2}]^-[Te(1)O_{2/2}O_{2/3}]^{+0.666}[Te(2)O_{4/3}]^{+1.333}\}^0$ neutral framework in connectivity terms. Bond valence sum calculations[55,56] for In^{3+}, Nb^{5+}, Te^{4+}, and O^{2-} in $InNb(TeO_4)_2$ show values of 2.80, 4.96, 4.04−4.18, and 1.81−2.12, respectively.

Infrared Spectroscopy. In−O, Nb−O, and Te−O vibrations are found in the infrared spectrum for $InNb(TeO_4)_2$. The In−O and Nb−O vibrations occur in the regions ca. 442−462 and 514−597 cm^{-1}, respectively. Multiple peaks observed around 624−771 cm^{-1} may be assigned to Te−O vibrations. The observed vibrational bands and their assignments are summarized in Table 3, which are consistent with the vibrations of previously reported oxide materials.[38,57,58] In addition, the infrared spectrum for $InNb(TeO_4)_2$ is placed in the Supporting Information.

Table 3. Infrared Vibrations (cm^{-1}) for $InNb(TeO_4)_2$

In−O	Nb−O	Te−O
447	514	624
462	597	651
		684
		744
		771

UV−Vis Diffuse Reflectance Spectroscopy. The UV−vis diffuse reflectance spectrum of $InNb(TeO_4)_2$ has been obtained and the following Kubelka−Munk function was used to calculate absorption (*K*/*S*) data:[52,53]

$$F(R) = \frac{(1-R)^2}{2R} = \frac{K}{S}$$

where *S* is the scattering, *R* is the reflectance, and *K* is the absorption. Extrapolation of the linear division of the ascending curve to 0 resulted in the absorption onset at 3.5 eV in the *K*/*S* vs *E* plot for $InNb(TeO_4)_2$ (see Figure 3). The band gap for $InNb(TeO_4)_2$ should be due to both of the distortions resulting from TeO_4 polyhedra and the degree of Nb (4d) orbitals involved in the conduction bands.

Thermogravimetric Analysis. Thermal analysis was performed to evaluate the thermal behavior of $InNb(TeO_4)_2$ under a flowing argon atmosphere from room temperature to 1000 °C. The reported material is thermally stable to 740 °C.

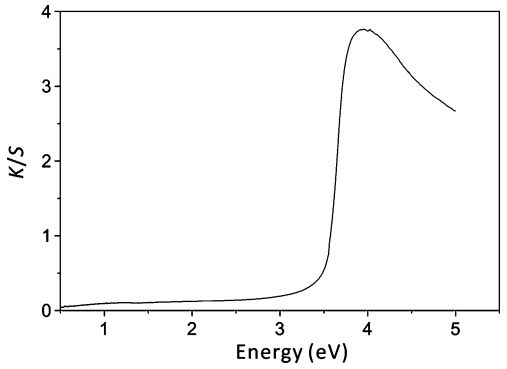

Figure 3. UV−vis diffuse reflectance spectrum of $InNb(TeO_4)_2$, revealing the absorption edge at 3.5 eV.

Above the temperature, thermal decomposition takes place and the material breaks down to a mixture of $InNbO_4$ (PDF #25-0384) and some amorphous phases as confirmed by the powder XRD measurement. The thermogravimetric analysis diagram and the PXRD pattern for the thermally decomposed material can be found in the Supporting Information.

Second-Order Nonlinear Optical (NLO) Measurements. $InNb(TeO_4)_2$ exhibits a polar NCS space group, $Pca2_1$; thus, its detailed second-order NLO properties have been examined. Powder SHG measurements, using 1064 nm radiation with a Kurtz-NLO system, show that $InNb(TeO_4)_2$ possesses a SHG efficiency 100 times that of α-SiO_2. If we compare the SHG efficiencies with those of some known NCS tellurites, $InNb(TeO_4)_2$ exhibits stronger SHG intensity than $Te_2O(PO_4)_2$ (50 × α-SiO_2)[31] or $Ga_2Zn(TeO_3)_4$ (40 × α-SiO_2).[59] When polycrystalline $InNb(TeO_4)_2$ was sieved into a variety of distinct particle sizes, ranging 20−150 μm, and the SHG was estimated with regard to particle size, the phase-matching (type 1) abilities of the compound could be resolved. $InNb(TeO_4)_2$ turned out to be nonphase-matchable, as seen in Figure 4.[54]

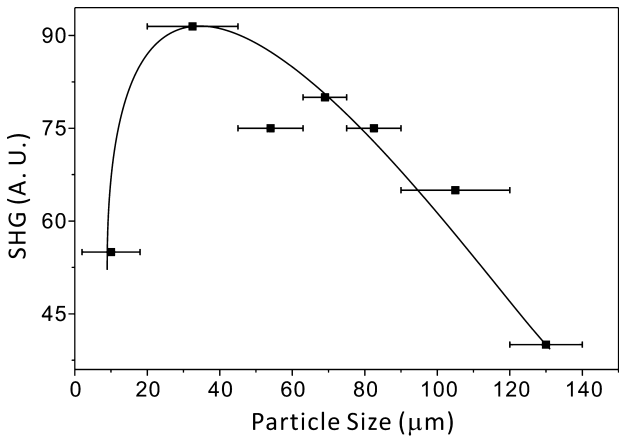

Figure 4. Type 1 phase-matching curve for $InNb(TeO_4)_2$. The curve is to guide the eye and is not a fit to the data.

Calculations of Out-of-Center Distortions and Dipole Moments. Because $InNb(TeO_4)_2$ contains a d^0 transition-metal cation, i.e., Nb^{5+}, with octahedral coordination, the extent of out-of-center distortion (Δ_d) for the NbO_6 octahedron has been determined. The method considers not only the six M−O bond lengths but also deviations of the three trans O−M−O

dx.doi.org/10.1021/ic5004337 | Inorg. Chem. 2014, 53, 5240−5245

bond angles from 180°.[15] The Δ_d value for NbO_6 octahedra in $InNb(TeO_4)_2$ can be calculated to be 0.70 using this methodology. The calculated value is similar to the average magnitude of the intraoctahedral distortion scale of 0.62 for Nb^{5+}.[15] In fact, on the basis of the calculated average Δ_d values for NbO_6 octahedra, Nb^{5+} is classified as a moderate distorter.

The reported NCS material contains two families of SOJT distortive cations, a lone pair cation (Te^{4+}) and an octahedrally coordinated d^0 transition-metal cation (Nb^{5+}). Since both cations exhibit asymmetric environments, the direction and extent of the distortions in the NbO_6 and TeO_4 polyhedra may be determined by calculating the local dipole moments. The method was reported before with regard to metal oxyfluoride octahedra through bond valence calculations.[60−62] The calculated local dipole moments for NbO_6 and TeO_4 in $InNb(TeO_4)_2$ are about 7.96 and 10.41−11.39 D, respectively, which are very similar to the published dipole moments of NbO_6 and TeO_4.[38]

Structure−SHG Property Relationships. As we described earlier, $InNb(TeO_4)_2$ reveals a SHG response 100 times that of α-SiO_2. The strong SHG efficiency can be interpreted by analyzing the net direction of the polarizations originating from individual asymmetric polyhedra. In $InNb(TeO_4)_2$, three different families of polyhedra such as InO_6, NbO_6, and TeO_4 exist; however, we assume that the octahedral moiety of InO_6 does not significantly contribute to the SHG properties, because the octahedra are not polar as are other polyhedra of SOJT cations. Then, other SOJT cations, Nb^{5+} and Te^{4+}, may provide notably to the SHG intensity attributed to the polarization originating from the noncentrosymmetric moiety. The Nb^{5+} cations distort along one of the local C_3 directions such as [−1−11], [−111], [1−11], and [111] attributable to out-of-center distortions of their corresponding octahedra (see Figure 5a). A net moment is generated in the [001] direction when taken as a whole. Also, the lone pairs on $Te(1)^{4+}$ point approximately along the [11−1], [−11−1], [1−1−1], and [−1−1−1] directions. When taken as a whole, another net moment associated with $Te(1)^{4+}$ is noticed pointing in the [001] direction because the local moment for the $Te(1)O_4$ occurs toward the opposite direction of the lone pair (see Figure 5b). In addition, the lone pairs on $Te(2)^{4+}$ point approximately in [010] and [0−10] directions. However, the lone pair polarizations related to $Te(2)^{4+}$ cancel if summed up. Thus, combining the moments as a whole, a net polarization of 18.37 D (approximately 43% from NbO_6 and 57% from TeO_4) is noted along the [001] direction on the basis of the dipole moment calculations for NCS $InNb(TeO_4)_2$, which is accountable for the strong SHG efficiency.

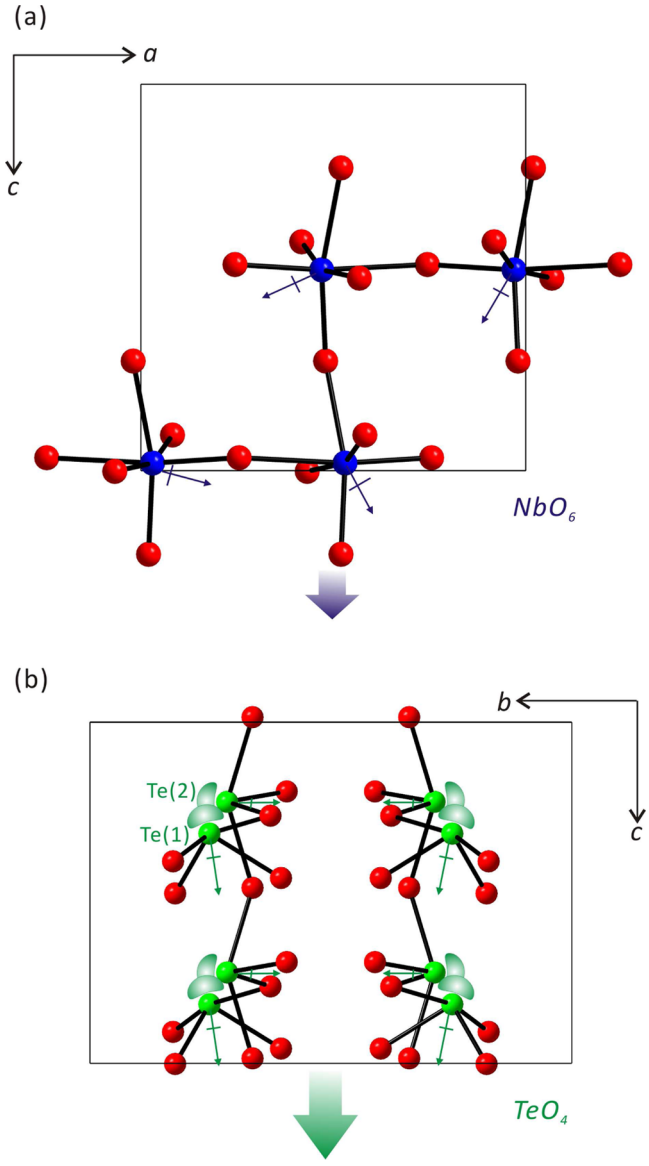

Figure 5. Ball-and-stick models representing moments arising from (a) out-of-center distortions of NbO_6 octahedra and (b) lone pairs of TeO_4 polyhedra in $InNb(TeO_4)_2$. When taken as a whole, a net moment is observed along the [001] direction, which is responsible for the strong SHG response.

CONCLUSIONS

Both pure bulk samples and single crystals of a new polar indium niobium tellurite material, $InNb(TeO_4)_2$, have been synthesized by standard solid-state reactions. Structural analysis indicates that the three-dimensional framework of $InNb(TeO_4)_2$ consists of layers of vertex-sharing InO_6, layers of corner-sharing NbO_6, and chains of corner-sharing TeO_4 polyhedra. Powder NLO measurements reveal that NCS $InNb(TeO_4)_2$ has an SHG response 100 times that of α-SiO_2. Close examinations of the structure−property relationships indicate that the strong SHG intensity of $InNb(TeO_4)_2$ is attributable to the combined net polarization arising from out-of-center distortions of NbO_6 octahedra as well as alignment of asymmetric $Te(1)^{4+}O_4$ polyhedra. Thermogravimetric analysis, infrared spectroscopy, UV−vis diffuse reflectance spectroscopy, dipole moment calculations, and calculations of octahedral distortion were also carried out for the presented material.

ASSOCIATED CONTENT

Supporting Information

A CIF file giving X-ray crystallographic data and figures giving X-ray diffraction patterns, a thermogravimetric analysis diagram, and an infrared spectrum for $InNb(TeO_4)_2$. This material is available free of charge via the Internet at http://pubs.acs.org.

AUTHOR INFORMATION

Corresponding Author

*K.M.O.: e-mail, kmok@cau.ac.kr; tel, +82-2-820-5197, fax, +82-2-825-4736.

Notes

The authors declare no competing financial interest.

dx.doi.org/10.1021/ic5004337 | Inorg. Chem. 2014, 53, 5240−5245

■ ACKNOWLEDGMENTS

This work was supported by the Basic Science Research Program through the National Research Foundation of Korea (NRF) funded by the Ministry of Education, Science & Technology (Grant No. 2013R1A2A2A01007170).

■ REFERENCES

(1) Nye, J. F. *Physical Properties of Crystals*; Oxford University Press: Oxford, U.K., 1957.
(2) Jona, F.; Shirane, G. *Ferroelectric Crystals*; Pergamon Press: Oxford, U.K., 1962.
(3) Cady, W. G. *Piezoelectricity; an Introduction to the Theory and Applications of Electromechanical Phenomena in Crystals*; Dover: New York, 1964; p 822.
(4) Lang, S. B. *Sourcebook of Pyroelectricity*; Gordon & Breach Science: London, 1974.
(5) Halasyamani, P. S.; Poeppelmeier, K. R. *Chem. Mater.* **1998**, *10*, 2753−2769.
(6) Ok, K. M.; Chi, E. O.; Halasyamani, P. S. *Chem. Soc. Rev.* **2006**, *35*, 710−717.
(7) Lee, D. W.; Ok, K. M. *Solid State Sci.* **2010**, *12*, 2036.
(8) Opik, U.; Pryce, M. H. L. *Proc. R. Soc. London* **1957**, *A238*, 425−447.
(9) Bader, R. F. W. *Can. J. Chem.* **1962**, *40*, 1164−1175.
(10) Pearson, R. G. *J. Am. Chem. Soc.* **1969**, *91*, 4947−4955.
(11) Pearson, R. G. *J. Mol. Struct. (THEOCHEM)* **1983**, *103*, 25−34.
(12) Wheeler, R. A.; Whangbo, M.-H.; Hughbanks, T.; Hoffmann, R.; Burdett, J. K.; Albright, T. A. *J. Am. Chem. Soc.* **1986**, *108*, 2222−2236.
(13) Kunz, M.; Brown, I. D. *J. Solid State Chem.* **1995**, *115*, 395−406.
(14) Oh, S.-J.; Lee, D. W.; Ok, K. M. *Dalton Trans.* **2012**, *41*, 2995−3000.
(15) Halasyamani, P. S. *Chem. Mater.* **2004**, *16*, 3586−3592.
(16) Lefebvre, I.; Lannoo, M.; Allan, G.; Ibanez, A.; Fourcade, J.; Jumas, J. C. *Phys. Rev. Lett.* **1987**, *59*, 2471−2474.
(17) Lefebvre, I.; Szymanski, M. A.; Olivier-Fourcade, J.; Jumas, J. C. *Phys. Rev. B* **1998**, *58*, 1896−1906.
(18) Watson, G. W.; Parker, S. C. *J. Phys. Chem. B* **1999**, *103*, 1258−1262.
(19) Watson, G. W.; Parker, S. C.; Kresse, G. *Phys. Rev. B* **1999**, *59*, 8481−8486.
(20) Seshadri, R.; Hill, N. A. *Chem. Mater.* **2001**, *13*, 2892−2899.
(21) Waghmare, U. V.; Spaldin, N. A.; Kandpal, H. C.; Seshadri, R. *Phys. Rev. B* **2003**, *67*, 125111/1−125111/10.
(22) Walsh, A.; Payne, D. J.; Egdell, R. G.; Watson, G. W. *Chem. Soc. Rev.* **2011**, *40*, 4455−4463.
(23) Champarnaud-Mesjard, J. C.; Frit, B.; Chagraoui, A.; Tairi, A. *J. Solid State Chem.* **1996**, *127*, 248−255.
(24) Champarnaud-Mesjard, J. C.; Frit, B.; Chagraoui, A.; Tairi, A. *Z. Anorg. Allg. Chem.* **1996**, *622*, 1907−1912.
(25) Ok, K. M.; Orzechowski, J.; Halasyamani, P. S. *Inorg. Chem.* **2004**, *43*, 964−968.
(26) Zhang, Z.; Tao, X.; Zhang, J.; Sun, Y.; Zhang, C.; Li, B. *CrystEngComm* **2013**, *15*, 10197−10204.
(27) Alonso, J. A.; Castro, A.; Puebla, E. G.; Monge, M. A.; Rasines, I.; Valero, C. R. *J. Solid State Chem.* **1987**, *69*, 36−42.
(28) Ok, K. M.; Halasyamani, P. S. *Inorg. Chem.* **2002**, *41*, 3805−3807.
(29) Alcock, N. W.; Harrison, W. D. *Acta Crystallogr.* **1982**, *B38*, 1809−1811.
(30) Mayer, H.; Weil, M. *Z. Anorg. Allg. Chem.* **2003**, *629*, 1068−1072.
(31) Kim, M. K.; Kim, S.-H.; Chang, H.-Y.; Halasyamani, P. S.; Ok, K. M. *Inorg. Chem.* **2010**, *49*, 7028−7034.
(32) Chen, X. A.; Zhang, L.; Chang, X.; Xue, H.; Zang, H.; Xiao, W. Q.; Song, X.; Yan, H. *J. Alloys Compd.* **2007**, *428*, 54−58.
(33) Kong, F.; Hu, C.; Hu, T.; Zhou, Y.; Mao, J.-G. *Dalton Trans.* **2009**, 4962−4970.
(34) Yang, B.; Hu, C.; Xu, X.; Sun, C.; Zhang Jian, H.; Mao, J.-G. *Chem. Mater.* **2010**, *22*, 1545−1550.
(35) Oh, S.-J.; Lee, D. W.; Ok, K. M. *Inorg. Chem.* **2012**, *51*, 5393−5399.
(36) Galy, J.; Lindqvist, O. *J. Solid State Chem.* **1979**, *27*, 279−286.
(37) Blanchandin, S.; Champarnaud-Mesjard, J. C.; Thomas, P.; Frit, B. *J. Alloys Compd.* **2000**, *306*, 175−185.
(38) Ok, K. M.; Halasyamani, P. S. *Inorg. Chem.* **2005**, *44*, 3919−3925.
(39) Gu, Q.-H.; Hu, C.-L.; Zhang, J.-H.; Mao, J.-G. *Dalton Trans.* **2011**, *40*, 2562−2569.
(40) Wedel, B.; Mueller-Buschbaum, H. *Z. Naturforsch., B: J. Chem. Sci.* **1996**, *51*, 1407−1410.
(41) Wedel, B.; Mueller-Buschbaum, H. *Z. Naturforsch., B: J. Chem. Sci.* **1996**, *51*, 1411−1414.
(42) Blanchandin, S.; Champarnaud-Mesjard, J. C.; Thomas, P.; Frit, B. *Solid State Sci.* **2000**, *2*, 223−228.
(43) Ok, K. M.; Zhang, L.; Halasyamani, P. S. *J. Solid State Chem.* **2003**, *175*, 264−271.
(44) Lee, D. W.; Oh, S. J.; Halasyamani, P. S.; Ok, K. M. *Inorg. Chem.* **2012**, *50*, 4473.
(45) Kim, Y. H.; Lee, D. W.; Ok, K. M. *Inorg. Chem.* **2013**, *52*, 11450−11456.
(46) Kim, Y. H.; Lee, D. W.; Ok, K. M. *Inorg. Chem.* **2014**, *53*, 1250−1256.
(47) *SAINT, Program for Area Detector Absorption Correction; version 4.05*; Siemens Analytical X-ray Instruments, Madison, WI, USA, 1995.
(48) Blessing, R. H. *Acta Crystallogr., Sect. A: Found. Crystallogr.* **1995**, *A51*, 33−38.
(49) Sheldrick, G. M. *SHELXS-97: A program for automatic solution of crystal structures*; University of Göttingen: Göttingen, Germany, 1997.
(50) Sheldrick, G. M. *SHELXL-97: A program for crystal structure refinement*; University of Göttingen: Göttingen, Germany, 1997.
(51) Farrugia, L. J. *J. Appl. Crystallogr.* **1999**, *32*, 837−838.
(52) Kubelka, P.; Munk, F. *Z. Technol. Phys.* **1931**, *12*, 593.
(53) Tauc, J. *Mater. Res. Bull.* **1970**, *5*, 721−729.
(54) Kurtz, S. K.; Perry, T. T. *J. Appl. Phys.* **1968**, *39*, 3798−3813.
(55) Brown, I. D.; Altermatt, D. *Acta Crystallogr., Sect. B* **1985**, *B41*, 244−247.
(56) Brese, N. E.; O'Keeffe, M. *Acta Crystallogr., Sect. B* **1991**, *B47*, 192−197.
(57) Li, P. X.; Kong, F.; Hu, C. L.; Zhao, N.; Mao, J.-G. *Inorg. Chem.* **2010**, *49*, 5943−5952.
(58) Lee, D. W.; Kim, S. B.; Ok, K. M. *Inorg. Chem.* **2012**, *51*, 8530−8537.
(59) Lee, D. W.; Bak, D.-b.; Kim, S. B.; Kim, J.; Ok, K. M. *Inorg. Chem.* **2012**, *51*, 7844−7850.
(60) Galy, J.; Meunier, G. *J. Solid State Chem.* **1975**, *13*, 142−159.
(61) Maggard, P. A.; Nault, T. S.; Stern, C. L.; Poeppelmeier, K. R. *J. Solid State Chem.* **2003**, *175*, 27−33.
(62) Izumi, H. K.; Kirsch, J. E.; Stern, C. L.; Poeppelmeier, K. R. *Inorg. Chem.* **2005**, *44*, 884−895.